

On the Arnold cat map and periodic boundary conditions for planar elongational flow

THOMAS A. HUNT and B. D. TODD*

Centre for Molecular Simulation, Swinburne University of Technology,
PO Box 218, Hawthorn VIC 3122, Australia

(Received 18 September 2003; revised version accepted 17 November 2003)

In this paper we show that the periodic boundary conditions used to simulate planar elongational flow are closely related to the Arnold cat map. In particular the relationship between the Arnold cat map and the periodic boundary conditions devised by Kraynik and Reinelt [1992, *Int. J. multiphase Flow*, **18**, 1045], the so-called K-R map, is demonstrated. It is shown that the family of lattices found by Kraynik and Reinelt corresponds to a subset of hyperbolic toral automorphisms. These lattices were previously found to be sufficient to enable molecular dynamics simulations of steady-state planar elongational flow of unrestricted duration. Within the frame of the cat map we provide a re-derivation for the set of eigenvalues, eigenvectors and orientation angles of the K-R map and find it to be considerably simpler than the original derivation provided by Kraynik and Reinelt.

1. Introduction

Until very recently it was thought that dynamical simulations of planar elongational flow using techniques such as non-equilibrium molecular dynamics (NEMD) were impossible to perform for molecular systems due to the fact that this type of flow demands that the unit cell is compressed in at least one dimension. This in turn implies that simulations must cease once the length of the cell in the direction of compression reaches its minimum possible extent of twice the range of the interatomic potential radius. For simple atomic fluids this minimum extension can be feasibly reached well before the characteristic relaxation time of the fluid, allowing steady-state conditions to be satisfied and measurements to be made. For complex molecular fluids, such as polymer melts, the characteristic relaxation times are significantly longer than the time taken to reach the minimum extension of the simulation cell, and as such steady-state cannot be achieved. This was a severe limitation for such techniques, because elongational flow is in many ways more significant for the rheology of polymer materials than shear flow, which is relatively straightforward to simulate using standard NEMD techniques.

In 1992 Kraynik and Reinelt [1] found a set of lattices that were reproduced after a time τ_p when they underwent planar elongational flow. With extensive analysis they showed that similarly reproducible lattices did not exist for uniaxial or biaxial elongational flows.

It was later demonstrated [2–4] that the cells of these lattices may be used as the boundaries for simulation cells of a homogeneous non-equilibrium molecular dynamics simulation of planar elongational flow. These boundaries in turn are both spatially and temporally periodic. Their spatial periodicity ensures the system remains homogeneous in space, whereas the temporal periodicity allows NEMD simulations of unrestricted duration. This in turn has allowed the first simulations of long-chain polymer melts undergoing steady-state planar elongational flow [5–7].

In this paper we make the observation that the lattices found by Kraynik and Reinelt are closely related to the Arnold cat map [8], which is a simple area preserving map of the torus onto itself that has been studied extensively in the dynamical systems literature and is often used when discussing ergodicity [9, 10]. We also demonstrate how application of the cat map greatly simplifies the computation of the eigenvalues and eigenvectors of the lattices computed by Kraynik and Reinelt, as well as the alignment angles that such a spatio-temporally periodic simulation cell makes with respect to the flow fields.

2. The relationship between dynamical maps and periodic boundary conditions

In molecular dynamics simulations the time evolution of the positions and momenta of a system of atoms or molecules is calculated by numerically integrating suitable equations of motion. At equilibrium the suitable equations of motion are Hamilton's equations

*Author for correspondence. e-mail: btodd@swin.edu.au

or equivalently Newton's equation. However, fluid systems are almost never at equilibrium and one of the goals of non-equilibrium molecular dynamics has been to simulate systems of atoms and molecules with a macroscopic flow field $\mathbf{u}(\mathbf{r}, t)$ with constant shear or elongation gradients,

$$\nabla\mathbf{u}(\mathbf{r}, t) = \begin{pmatrix} \frac{\partial u_x}{\partial x} & \frac{\partial u_y}{\partial x} & \frac{\partial u_z}{\partial x} \\ \frac{\partial u_x}{\partial y} & \frac{\partial u_y}{\partial y} & \frac{\partial u_z}{\partial y} \\ \frac{\partial u_x}{\partial z} & \frac{\partial u_y}{\partial z} & \frac{\partial u_z}{\partial z} \end{pmatrix} = \begin{pmatrix} \dot{\epsilon} & 0 & 0 \\ \dot{\gamma} & -\dot{\epsilon} & 0 \\ 0 & 0 & 0 \end{pmatrix}. \quad (1)$$

Homogeneous flows with such flow fields are only possible with suitable periodic boundary conditions that are compatible with the flow geometry. In this paper we particularly consider the situation in which a system of particles undergoes planar elongational flow, in which $\dot{\gamma} = 0$ and $\dot{\epsilon} \neq 0$. For pedagogical purposes we first

consider the relationship between maps and periodic boundary conditions at equilibrium and under planar shear (or planar Couette) flow, as these two conditions are simpler to understand. Planar Couette flow occurs when $\dot{\epsilon} = 0$ and $\dot{\gamma} \neq 0$.

2.1. Equilibrium

An equilibrium molecular dynamics simulation at constant energy is simply implemented by integrating Newton's equations of motion for the time evolution of positions and momenta. One may of course simulate other ensembles, e.g. (N, V, T) , (N, p, T) , etc., by suitable perturbations to the equations of motion that involve the introduction of thermostats, barostats, etc. For the system to remain homogeneous in space one applies periodic boundary conditions, as depicted in figure 1. Figure 1 shows a simulation cell (denoted by the thick boundary square). The cells adjacent to the central simulation cell are periodic images of it. Particles that move out through

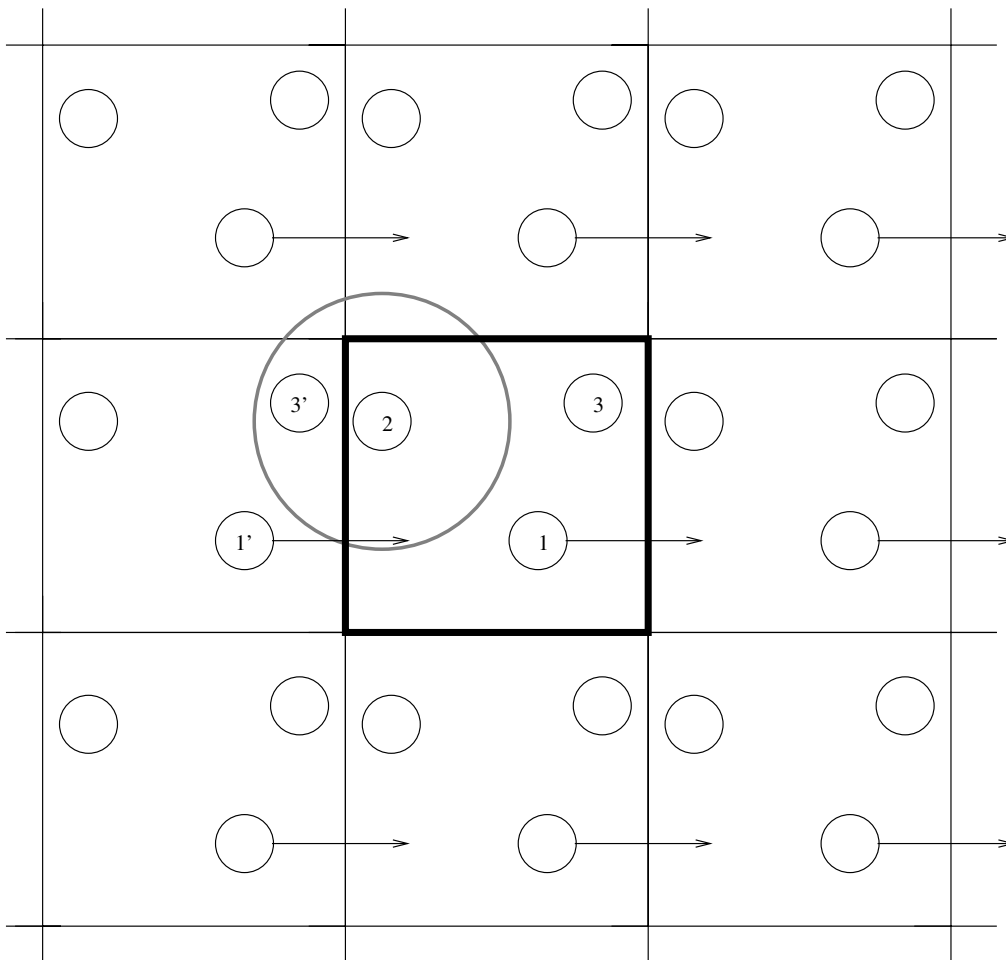


Figure 1. The square periodic boundary conditions commonly used for equilibrium molecular dynamics simulations. The central cell (bold) is the primary cell and the cells surrounding it are its periodic images. Particles 1' and 3' are periodic images of particles 1 and 3, respectively. Due to the minimum image convention atom 2 interacts with particle 3' and not particle 3.

one face of the cell are replaced by their images coming in through the opposite face. For example, in figure 1 particle 1 moves out of the right-hand face of the central simulation cell and is replaced by particle 1' coming in from the left image box. The interactions between particles are calculated such that an atom interacts with its closest image. Again referring to figure 1, atom 2 will interact with atom 3' instead of atom 3, since atom 3' is closer to atom 2 than atom 3.

The above example is well known and standard in the description of periodic boundary conditions for molecular dynamics simulations. What is not as well known is that these boundary conditions are equivalent to spatio-temporal mappings. A map is an operation that transforms the state of a system at time t to an allowable state at time $t + 1$. Maps have been particularly instrumental in our understanding of chaos in dynamical systems in recent years. A functional mapping may be defined as

$$\mathbf{x}_{t+1} = \mathbf{M}(\mathbf{x}_t), \quad (2)$$

where \mathbf{x} is an n -dimensional vector that describes the state of the system and \mathbf{M} is the mapping operation. For the case of an equilibrium MD system, such a mapping scheme for particle positions is

$$\begin{pmatrix} x' \\ y' \\ z' \end{pmatrix} = \begin{pmatrix} 1 & 0 & 0 \\ 0 & 1 & 0 \\ 0 & 0 & 1 \end{pmatrix} \begin{pmatrix} x \\ y \\ z \end{pmatrix} \text{ mod } (L), \quad (3)$$

where L is the length of the simulation cell.

Notice that the physical mapping of a particle with coordinates $\mathbf{x} = (x, y, z)$ into one with coordinates $\mathbf{x}' = (x', y', z')$ occurs due to the modulo operation. Only when particles move out of the simulation box does the modulo operation map these particles back into the box; otherwise particle positions remain unchanged by the mapping. The mapping operation depicted in equation (3) is thus equivalent to the scheme of periodic boundary conditions used in typical equilibrium MD simulations.

2.2. Shear flow

One technique for simulating planar Couette flow involves simulating a system of fluid particles confined between two solid walls composed of atoms [11], in which the lower wall remains fixed in space and the upper wall moves at constant velocity in the direction of shear, resulting in a uniform velocity profile in the fluid. By thermostating the two walls the system can be kept at a constant temperature for small shear rates. However at large shear rates the increase in internal energy cannot be compensated for by thermostating just the walls and

a temperature gradient results. Furthermore, the structure of the walls induces density gradients within the fluid such that the fluid is not spatially homogeneous. Both these reasons make such simulations problematic in understanding the transport processes of spatially homogeneous systems at constant temperature.

An alternative technique is to introduce a perturbation into the equations of motion that transform a boundary driven flow into one under the application of a smooth mechanical force. Known as the SLLOD equations of motion [12], they have been successful in simulating non-equilibrium flows that are spatially homogeneous. They can be coupled to appropriate time-reversible thermostats to remove excess viscous heat generated by the flow to guarantee the system remains at constant temperature.

The SLLOD equations of motion for a system of atoms undergoing isothermal planar Couette flow are

$$\begin{aligned} \dot{\mathbf{r}}_i &= \frac{\mathbf{p}_i}{m_i} + \dot{\gamma} y_i \hat{\mathbf{i}}, \\ \dot{\mathbf{p}}_i &= \mathbf{F}_i - \dot{\gamma} p_{iy} \hat{\mathbf{i}} - \zeta \mathbf{p}_i, \end{aligned} \quad (4)$$

where $\mathbf{r}_i = (x_i, y_i, z_i)$ is the laboratory position of atom i with peculiar (i.e. thermal) momentum $\mathbf{p}_i = (p_{ix}, p_{iy}, p_{iz})$ and mass m_i . $\hat{\mathbf{i}}$ is the unit vector in the x direction and $\dot{\gamma}$ is the shear rate for the system being simulated. The force on atom i due to the surrounding atoms is \mathbf{F}_i and is dependent on the chemical nature of the system, while ζ is an atomic thermostat that may be given in the Gaussian form [12] by

$$\zeta = \frac{\sum_{i=1}^N (\mathbf{F}_i \cdot \mathbf{p}_i - \dot{\gamma} p_{ix} p_{iy})}{\sum_{i=1}^N \mathbf{p}_i^2}. \quad (5)$$

Along with the equations of motion an essential component of the simulation algorithm is the periodic boundary conditions. For simulations of planar Couette flow the boundary conditions are no longer stationary but become periodic in time. In the Lees–Edwards scheme of periodic boundary conditions [13] shown in figure 2, periodic images above the primary cell slide with the velocity $+\dot{\gamma}L$ while the images below slide with velocity $-\dot{\gamma}L$. The initial condition of the system of cell and images is the stationary periodic boundary conditions for the simulation of an equilibrium system. Now because of the motion of the cells above and below the primary cell, the x component of the position of a particle must be adjusted by an amount $\pm \dot{\gamma}L \Delta t$, where Δt is the integration time step. For example, if particle 2 moves through the cell at the top interface, it re-emerges through the bottom interface shifted by an amount $-\dot{\gamma}L \Delta t$.

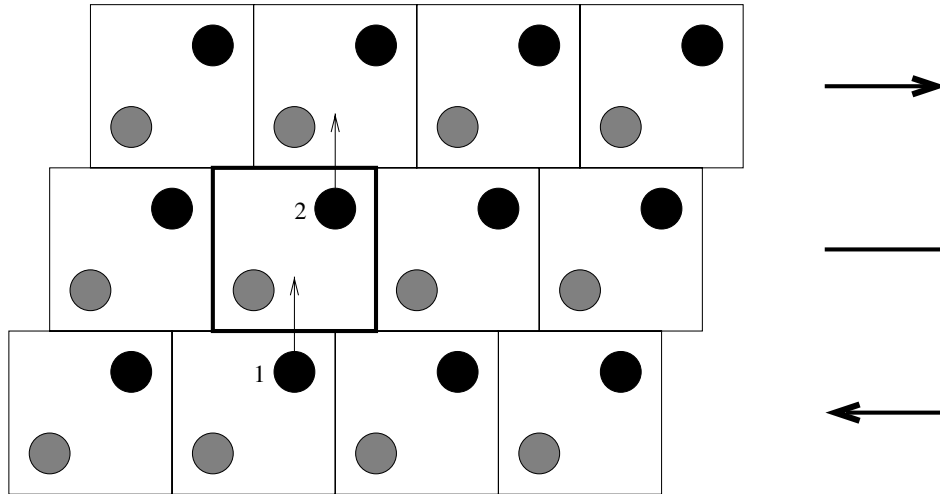


Figure 2. Lees-Edwards ‘sliding brick’ periodic boundary conditions for planar Couette flow. When particle 2 moves out of the top of the central cell (bold) it re-emerges through the bottom of the cell shifted in the x direction by an amount $-\dot{\gamma}L\Delta t$.

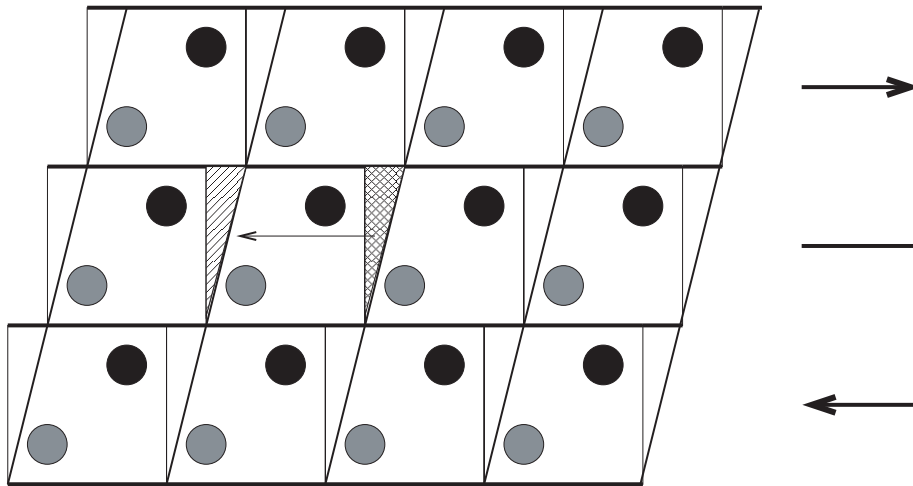


Figure 3. The Lagrangian-Rhomboid scheme for NEMD simulations of planar Couette flow. The equivalence of this scheme with the sliding brick scheme of figure 2 can be seen by chopping the right cross-hatched triangular section from the primary cell, shifting it by an amount $-L$ in the x direction, and re-inserting it into the left striped triangular section. Both schemes preserve the relative spatial separations between all particles exactly.

The periodic boundary conditions described above are termed ‘sliding brick’ because images of the simulation cell slide above and below it. An equivalent representation is the Lagrangian-Rhomboid scheme [14]. In this scheme the simulation cell deforms with the flow so that if the initial cell is the square $(x, y, z)^T \in [0, L] \times [0, L] \times [0, L]$ then at time t the primary cell is given by

$$\begin{pmatrix} x' \\ y' \\ z' \end{pmatrix} = \begin{pmatrix} 1 & \dot{\gamma}t & 0 \\ 0 & 1 & 0 \\ 0 & 0 & 1 \end{pmatrix} \begin{pmatrix} x \\ y \\ z \end{pmatrix}. \quad (6)$$

An instantaneous configuration of the cell and its periodic images is given in figure 3. If τ_p is the time period of the mapping, then at time $t = \tau_p = 1/\dot{\gamma}$ the

cell is mapped back to the original square cell. As in the case of the equilibrium mapping, this *non-equilibrium* mapping is achieved by using the modulo operation. Between $t = 0$ and $t = \tau_p$ the overall displacement of particles due to the streaming velocity is given by the map

$$\begin{pmatrix} x' \\ y' \end{pmatrix} = \begin{pmatrix} 1 & 1 \\ 0 & 1 \end{pmatrix} \begin{pmatrix} x \\ y \end{pmatrix} \text{ mod } (L), \quad (7)$$

where we note that as there is no flow in the z direction the non-equilibrium subset of the complete three-dimensional mapping need only be described by a two-dimensional matrix. Note that even though there is no flow in the y direction, the y coordinate *does* appear

in the mapped x coordinate (i.e. x'). This mapping is depicted in figure 4 with regions shaded to show how they transform. An important feature to note is that the elements of the matrix are integers so that the transformed cell maps exactly over the original cell. The boundary conditions for planar Couette flow are thus not only spatially periodic but also periodic in time. It is also of note that molecular dynamics simulations that utilize such spatio-temporal periodic boundary conditions are actually non-autonomous [15]; as such there is no way which any simulation of this type can be truly 'steady-state'. For most simulations of this sort, however, the system size is sufficiently large that the time and space periodicity inherent in the periodic boundary conditions is negligible.

2.3. Planar elongational flow

The previous section summarized how a system undergoing planar Couette flow can be simulated using the SLLOD equations of motion and suitably chosen periodic boundary conditions, and how these boundary conditions are related to an appropriate

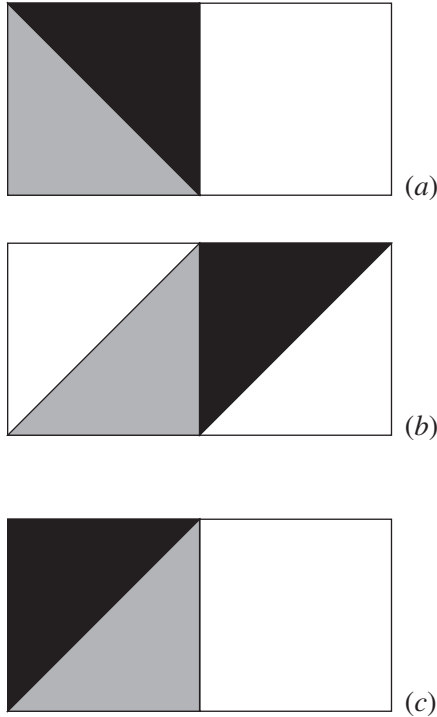


Figure 4. A diagram of the map used with Lagrangian–Rhomboid periodic boundary conditions in molecular dynamics simulations of planar Couette flow. Shading represents different regions of the map for clarity of visualization. (a) The initial configuration of the map, in the unit square. (b) The transformed map. (c) The transformed region is mapped back into the unit square.

dynamical map. The corresponding SLLOD equations of motion for planar elongational flow are [2, 3]

$$\begin{aligned}\dot{\mathbf{r}}_i &= \frac{\mathbf{p}_i}{m_i} + \dot{\varepsilon}(x_i\hat{\mathbf{i}} - y_i\hat{\mathbf{j}}), \\ \dot{\mathbf{p}} &= \mathbf{F}_i - \dot{\varepsilon}(x_i\hat{\mathbf{i}} - y_i\hat{\mathbf{j}}) - \zeta\mathbf{p}_i,\end{aligned}\quad (8)$$

where $\hat{\mathbf{i}}$ and $\hat{\mathbf{j}}$ are unit vectors in the x and y directions respectively and the Gaussian thermostat in this case is given by

$$\zeta = \frac{\sum_{i=1}^N (\mathbf{F}_i \cdot \mathbf{p}_i - \dot{\varepsilon}(p_{ix}^2 - p_{iy}^2))}{\sum_{i=1}^N \mathbf{p}_i^2}.\quad (9)$$

Given the equations of motion it is necessary to find a suitable set of periodic boundary conditions. As explained in the introduction, simple 'square' periodic boundary conditions are severely limited because ultimately the simulation must cease once the length of the cell in the contracting direction reaches its minimum extension of twice the range of the interatomic potential radius.

Kraynik and Reinelt [1] demonstrated how the extensional motion of spatially periodic lattices could be generated by suitable geometric orientations of the axes of the lattice with respect to the orientation of the elongating field. As described above and in [2–4], such periodic lattices may be used as the boundaries of a periodic simulation cell. In their derivation Kraynik and Reinelt [1] first construct an arbitrary lattice consisting of points $\mathbf{L}_i(t)$ governed by the dynamical equation

$$\begin{aligned}\mathbf{L}_i(t) &= \mathbf{N}(t) \cdot \mathbf{L}_i(0) \\ &= N_{i1}(t)\mathbf{L}_1(0) + N_{i2}(t)\mathbf{L}_2(0) + N_{i3}(t)\mathbf{L}_3(0).\end{aligned}\quad (10)$$

$\mathbf{L}_i(0)$ are the initial linearly independent basis lattice vectors, $\mathbf{N}(t) = \exp(\nabla\mathbf{u}t)$ is the matrix that describes the evolution with time of these basis vectors, $\nabla\mathbf{u}$ is the strain rate tensor and \mathbf{u} is the streaming fluid velocity. For a lattice to be reproducible (i.e. periodic in space and time), the constants $N_{ij}(t)$ must be integers at some time $t = \tau_p$. Kraynik and Reinelt then determined which sets of integers $N_{ij}(\tau_p)$ make equation (10) valid for a variety of extensional flows described by $\nabla\mathbf{u}$. These integers define the mapping, hereafter termed the K-R map. In turn, this reduces to the solution of an eigenvalue problem with corresponding eigenvectors. For the case of planar elongational flow, described by

$$\nabla\mathbf{u} = \begin{pmatrix} \dot{\varepsilon} & 0 & 0 \\ 0 & -\dot{\varepsilon} & 0 \\ 0 & 0 & 0 \end{pmatrix},\quad (11)$$

the eigenvalues were shown to be

$$\lambda_1 = \frac{k + (k^2 - 4)^{1/2}}{2}; \quad \lambda_2 = \lambda_1^{-1} = \frac{k - (k^2 - 4)^{1/2}}{2}, \quad (12)$$

where k is an integer with allowable values $k \geq 3$. Note that not all values of k are allowed, although there are an infinite number of them.

The directions of the two orthogonal eigenvectors (\mathbf{e}_1 and \mathbf{e}_2) in turn define the directions of the expanding and compressing fields with respect to the orientation of the basis vectors of the square lattice. If the x axis is chosen as the direction of expansion (at a rate $\dot{\epsilon}$), and the y axis is thus the direction of contraction (at a rate $-\dot{\epsilon}$), then the angle between \mathbf{e}_1 (parallel to the x axis) and the lattice basis vector \mathbf{b}_1 is the orientation angle θ (see figure 5 as well as figure 1 in [2]). There are an infinite number of these ‘magic’ angles which the initial lattice (or, equivalently, simulation cell) can be aligned with respect to the flow fields that guarantees the simulation cell is infinitely periodic in both space and time. As demonstrated above in the discussion of periodic boundary conditions for shear flow, it is this spatio-temporal periodicity, coupled with the SLLOD equations of motion, which allows one to perform NEMD simulations of spatially homogeneous flow indefinitely.

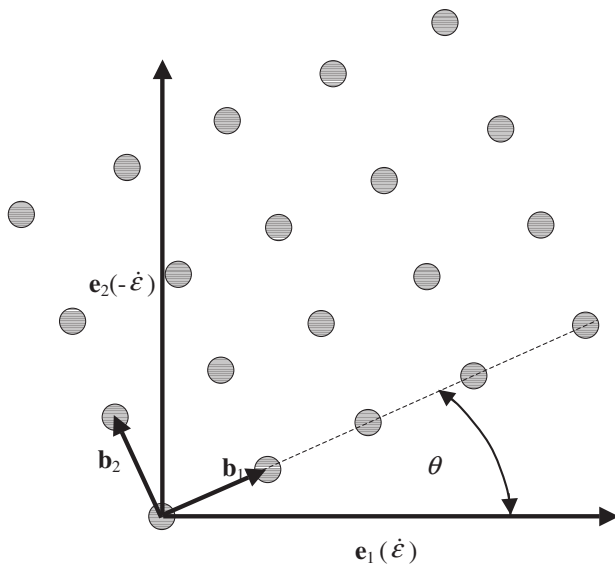


Figure 5. Alignment of lattice basis vectors \mathbf{b}_1 and \mathbf{b}_2 with eigenvectors \mathbf{e}_1 and \mathbf{e}_2 as performed in [2, 3] for NEMD simulations. \mathbf{e}_1 is parallel to the x axis and is the direction of elongation ($\dot{\epsilon}$) while \mathbf{e}_2 is parallel to the y axis and is the direction of compression ($-\dot{\epsilon}$). The orientation angle is that angle between \mathbf{e}_1 and \mathbf{b}_1 .

If τ_p is the lattice strain period, then the actual mapping of the extended simulation cell back into its original cell shape occurs when the value of the strain, $\epsilon = \dot{\epsilon}\tau_p$, equals the Hencky strain [1], ϵ_p . This is demonstrated in figure 6.

The original derivation of the eigenvalues, eigenvectors and orientation angles, while complete, is algebraically involved. In fact, Kraynik and Reinelt [1] assist readers with tables of orientation angles and relevant matrix integers $N_{ij}(\tau_p)$ for square (up to $k = 51$) and hexagonal (up to $k = 148$) lattices undergoing planar elongational flow. In the next section, we show how these periodic lattices are directly related to the Arnold cat map, and demonstrate a simplified approach to computing the eigenvalues, eigenvectors and orientation angles.

3. The Arnold cat map and Kraynik–Reinelt boundary conditions

The usual Arnold cat map is a map of the torus $\mathbb{T}^2 = \mathbb{R}^2/\mathbb{Z}^2$ onto itself

$$\begin{pmatrix} x' \\ y' \end{pmatrix} = \begin{pmatrix} 1 & 1 \\ 1 & 2 \end{pmatrix} \begin{pmatrix} x \\ y \end{pmatrix} \text{ mod } (1). \quad (13)$$

In this representation of the cat map, expansion takes place in the eigendirection \mathbf{e}_1 and contraction occurs in the eigendirection \mathbf{e}_2 (see figure 7). Thus the cat map ‘flow’ geometry is the opposite of the flow geometry employed by Kraynik and Reinelt and subsequent NEMD simulations of planar elongational flow [2–4].

The map described by equation (13) has two eigenvalues,

$$\lambda_1 = \frac{3 + 5^{1/2}}{2} > 1, \quad \lambda_1^{-1} = \lambda_2 = \frac{3 - 5^{1/2}}{2} < 1. \quad (14)$$

These eigenvalues are equivalent to those found by Kraynik and Reinelt, whose general solution is given in equation (12). Equation (14) is satisfied for $k = 3$ in equation (12). For the cat map, this corresponds to an alignment of the direction of expansion (in this case, parallel to the eigenvector, \mathbf{e}_1) at an angle of $\theta = 31.7^\circ$ with respect to the y axis (equivalent to the angle formed between \mathbf{e}_2 and the x axis). Any other allowable values of k may be used, and as previously noted there are an infinite number of them. They in turn correspond to hyperbolic toral automorphisms, which in turn are a set of Anosov diffeomorphisms [9]. Since the map is area preserving, the product of any set of eigenvalue

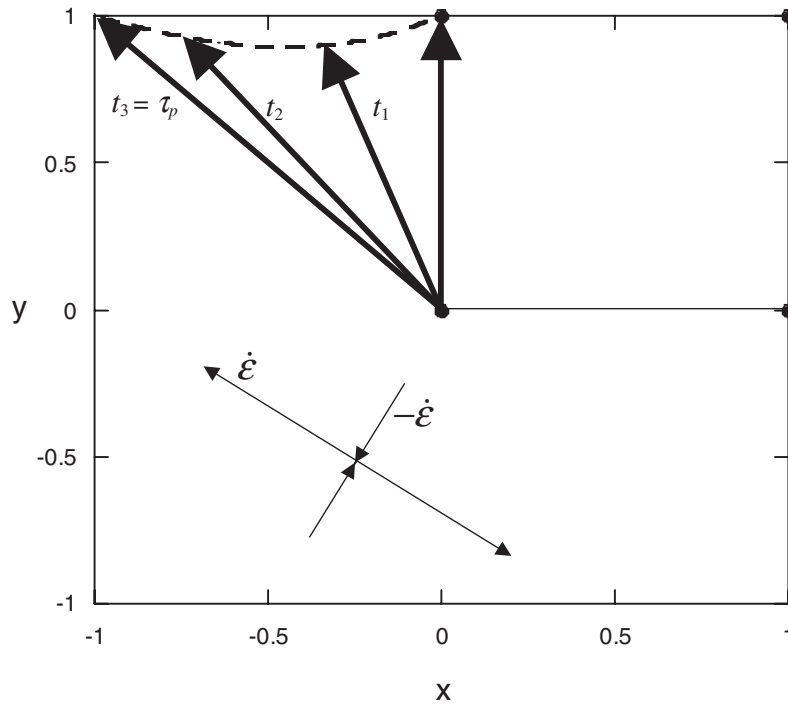


Figure 6. Mapping of simulation cell boundaries using the K-R map. The simulation cell boundaries are confined within the corners (0, 0), (0, 1), (1, 1) and (1, 0). The evolution of the boundary vector $\mathbf{x}_{01}(t = 0) = (0, 1)$ is depicted at various times, t_1 , t_2 and t_3 . At time $t_3 = \tau_p$ (the lattice strain period) \mathbf{x}_{01} has evolved to $(-1, 1)$. The K-R map now transforms this vector back into the original vector $\mathbf{x}_{01}(t = \tau_p) \rightarrow \mathbf{x}_{01}(t = 0) = (0, 1)$. The directions of expansion and compression are shown. The other three boundary vectors evolve in a similar manner. Note that this representation is equivalent to that used in the NEMD simulations of [2, 3]. In these simulations the directions of expansion and compression were the x and y axes respectively. Consequently the simulation cell was rotated by the orientation angle θ with respect to the x axis.

pairs is 1. The eigenvectors of the map described by equation (13) are

$$\mathbf{e}_1 = \begin{pmatrix} s \\ \frac{5^{1/2} + 1}{2}s \end{pmatrix}, \quad \mathbf{e}_2 = \begin{pmatrix} s \\ \frac{-5^{1/2} + 1}{2}s \end{pmatrix}, \quad (15)$$

where s is a real number. For convenience we set $s = 1$.

We note here that the Arnold cat map transformation is equivalent to the mapping that takes place in the Kraynik–Reinelt lattice when the Hencky strain, $\epsilon_p = \dot{\epsilon}\tau_p$, is attained, and we have already noted that it is this mapping which makes the Kraynik–Reinelt system reproducible, and hence periodic in time as well as space.

We give a diagram of the map described by equation (13) in figure 7. The relevant region starts as a unit square, figure 7(a), and is transformed to a parallelogram, figure 7(b), under the action of the integer matrix. The action of the modulo operation maps the transformed region back to the unit square, figure 7(c). Alternatively, one can view the modulo operation as being inherent due to the periodicity of

the torus. The shading in the diagram helps to show how different regions transform.

The example given in equation (13) is not a unique example of this type of map. The matrix in equation (13) can be replaced by any integer matrix with non-unit eigenvalues and positive or negative unit determinant. These maps are known as hyperbolic toral automorphisms, which in turn are a set of Anosov diffeomorphisms [9]. The family of lattices found by Kraynik and Reinelt [1] corresponds to a subset of hyperbolic toral automorphisms. The simplest of these, and the map chosen in the molecular dynamics simulations discussed earlier, is

$$\begin{pmatrix} x' \\ y' \end{pmatrix} = \begin{pmatrix} 2 & -1 \\ -1 & 1 \end{pmatrix} \begin{pmatrix} x \\ y \end{pmatrix} \text{ mod } (1). \quad (16)$$

This map is depicted in figure 8 and again areas are shaded to show how they transform. The eigenvalues of this map are the same as those of the usual Arnold cat map, while the eigenvectors are swapped, making this map the inverse of the cat map. This can be observed by inspecting the initial and final configurations of the two

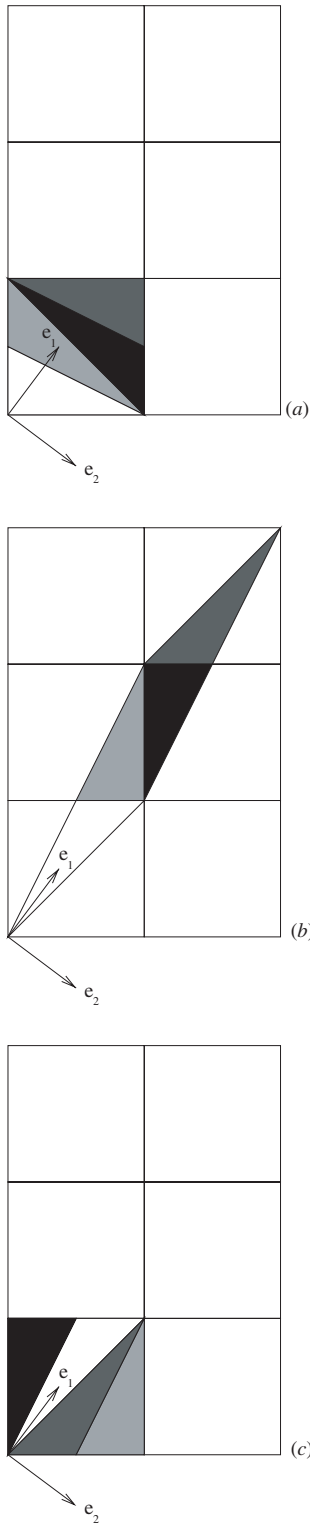


Figure 7. A diagram of the usual Arnold cat map. The vectors e_1 and e_2 give the expanding and contracting directions of the map respectively. Shading represents different regions of the map for clarity of visualization. (a) The initial configuration of the map, in the unit square. (b) The transformed map. (c) The transformed region is mapped back to the unit square.

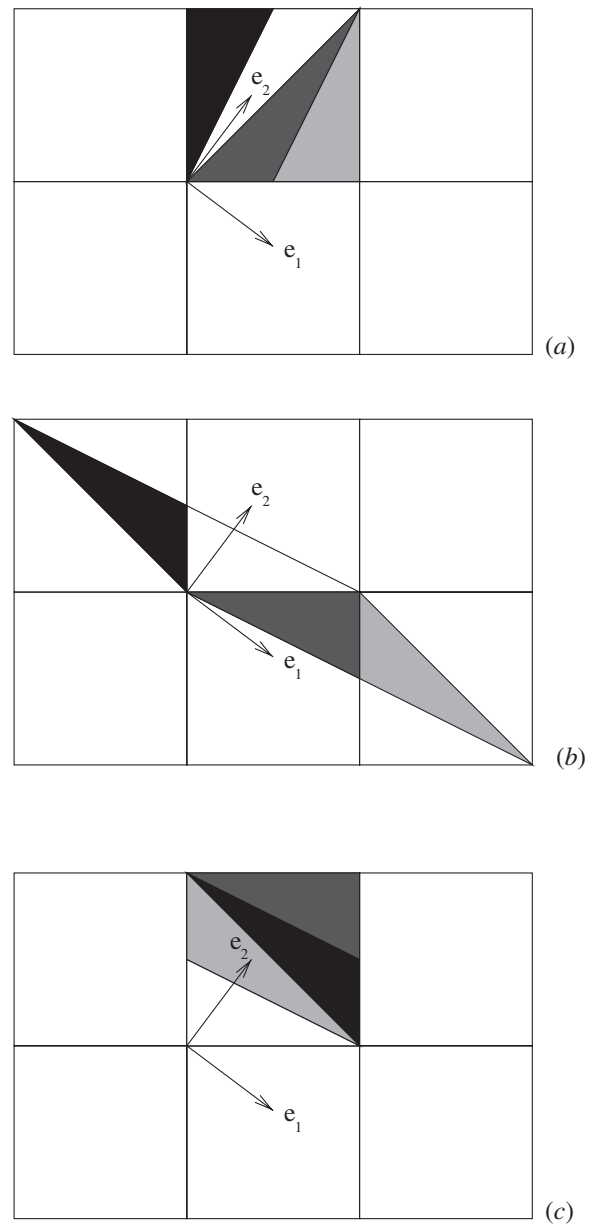


Figure 8. A diagram of the Kraynik–Reinelt map used in molecular dynamics simulations. The vectors e_1 and e_2 give the expanding and contracting directions of the map respectively. Shading represents different regions of the map for clarity of visualization. (a) The initial configuration of the map, in the unit square. (b) The transformed map. (c) The transformed region is mapped back to the unit square.

maps shown in figures 7 and 8, and comparing figures 6 and 8. At the beginning of the NEMD simulations the cell is rotated so that the extension and compression axes align with the x and y axes respectively [2, 3].

We now demonstrate that it is far simpler to compute the eigenvalues, eigenvectors and orientation angles from the cat map formalism, rather than the method

employed by Kraynik and Reinelt [1]. Consider the set of Anosov diffeomorphisms with the mapping

$$\mathbf{x}' = \mathbf{M}(\mathbf{x}), \tag{17}$$

where

$$\mathbf{M} = \begin{pmatrix} m_1 & m_2 \\ m_2 & m_3 \end{pmatrix} \tag{18}$$

is symmetric and $m_1, m_2, m_3 \in \mathbb{Z}$. These mappings are characterized by integer matrix elements and have the constraint imposed on them that they are area preserving, i.e.

$$\det(\mathbf{M}) = m_1 m_3 - m_2^2 = \pm 1. \tag{19}$$

In this work we do not consider the $\det(\mathbf{M}) = -1$ case, since it corresponds to a mapping which does not preserve the orientation of the mapped region and is therefore not useful for simulations. The eigenvalue equation for the map equation (17) is

$$\det(\lambda \mathbf{I} - \mathbf{M}) = 0, \tag{20}$$

which, when solved on substituting in equation (19) for the case $\det(\mathbf{M}) = +1$, gives the pair of eigenvalues

$$\lambda = \frac{(m_1 + m_3) \pm [(m_1 + m_3)^2 - 4]^{1/2}}{2}. \tag{21}$$

Comparison with equation (14) for the K-R map shows that $k = \text{Tr}(\mathbf{M})$. The Hencky strain is simply computed as $\varepsilon_p = \ln(\lambda)$ [1].

The eigenvectors of \mathbf{M} may now be trivially computed from the set of linear equations

$$\mathbf{M}\mathbf{x} = \lambda\mathbf{x} \tag{22}$$

giving us

$$\mathbf{e}_1 = \begin{pmatrix} s \\ (\frac{\lambda_1 - m_1}{m_2})s \end{pmatrix}, \quad \mathbf{e}_2 = \begin{pmatrix} s \\ (\frac{\lambda_2 - m_1}{m_2})s \end{pmatrix}. \tag{23}$$

Once again, we set $s = 1$ for convenience. We note that $m_2 = 0$ does not correspond to an Anosov diffeomorphism.

We denote the unit vector in the x direction as $\hat{\mathbf{x}}$ for the flow geometry adopted in figures 6 and 8. The orientation angle (i.e. the angle between the expanding direction and the x axis) can be thus simply computed from

$$\mathbf{e}_1 \cdot \hat{\mathbf{x}} = \|\mathbf{e}_1\| \|\hat{\mathbf{x}}\| \cos \theta, \tag{24}$$

i.e.

$$\theta = \cos^{-1} \left(\frac{1}{\|\mathbf{e}_1\|} \right). \tag{25}$$

In fact, it is clear that the matrix elements $N_{11}(\tau_p)$, $N_{12}(\tau_p)$, $N_{21}(\tau_p)$ and $N_{22}(\tau_p)$ in the K-R map are equivalent to m_3, m_2, m_2 and m_1 , respectively. However, our derivation of the eigenvalues, eigenvectors and orientation angles is somewhat more straightforward and simpler to that worked out in [1]. In particular, it is the orientation angle and Hencky strain (hence, strain period) that are of central importance in the practical implementation of the K-R map in NEMD simulations [2, 3].

As an example, consider the map

$$M = \begin{pmatrix} 5 & -2 \\ -2 & 1 \end{pmatrix}.$$

It has eigenvalues $\lambda = 3 \pm 2(2^{1/2})$ and eigenvectors

$$\mathbf{e}_1 = \begin{pmatrix} 1 \\ 1 - 2^{1/2} \end{pmatrix}$$

and

$$\mathbf{e}_2 = \begin{pmatrix} 1 \\ 1 + 2^{1/2} \end{pmatrix}.$$

The Hencky strain ($\ln \lambda$) is thus 1.76275 and the orientation angle (from equation (25)) is $\theta = 22.5^\circ$. Use of the cat map formalism determines these useful quantities in several lines of trivial algebra, compared to pages of algebra following the Kraynik–Reinelt procedure.

It can be shown that the rational points

$$\begin{pmatrix} \frac{p}{q} \\ \frac{r}{s} \end{pmatrix}; \quad p, q, r, s \in \mathbb{Z} \tag{26}$$

are periodic, and while this may induce artificial correlations when simulating a solid, correlations are unlikely to be noticeable when dealing with a fluid system which even at equilibrium has a relatively short correlation time.

In a further investigation [16] it was found that the use of Kraynik–Reinelt periodic boundary conditions was inherently unstable for very long simulations, and that momentum was not conserved in the direction of contraction. The total linear momentum in the contracting direction was found to grow exponentially in

time, leading to a catastrophic failure of the algorithm at long times. This exponential growth was due to numerical imprecision in the zeroing of the initial momentum necessary for conservation of momentum to prevail at all times. To counter this it was demonstrated [16] that one could either use a constraint mechanism to keep the total momentum constant, or alternatively one could periodically zero the centre-of-mass momentum. The source of this instability is equivalent to that described by McCauley [17] who, in his discussion of the Arnold cat map, points out that when simulating the Arnold cat map on a computer, numerical accuracy decreases exponentially with each application of the map. The implication is that for highly accurate results one is required to deal with numbers with many decimal places, and that the degree of accuracy is limited by the length of the simulation desired (i.e. the number of iterations required).

4. Conclusion

It had previously been demonstrated [2–4] that the periodic lattices in extensional flows first derived by Kraynik and Reinelt [1] may be used as periodic boundary conditions for non-equilibrium molecular dynamics simulations of planar elongational flow. In this paper we have shown that these periodic boundary conditions (the so-called K-R map) are in fact equivalent to the well-known cat map devised by Arnold [8] and used extensively in the study of dynamical systems. We have further demonstrated the simplicity of computing the eigenvalues, eigenvectors and orientation angles of this map with the intention of simplifying the much more algebraically involved derivation of those same quantities in [1].

Given the popularity of the Arnold cat map as an example of a chaotic map, it is of note that it also turns out to be an ideal choice of periodic boundary conditions for molecular dynamics simulations of planar elongational flow. These periodic boundary conditions

have now enabled us to simulate such flows for indefinite times, a feat previously considered impossible.

We thank Professor Denis Evans for reading the manuscript and providing useful suggestions.

References

- [1] KRAYNIK, A. M., and REINELT, D. A., 1992, *Int. J. multiphase Flow*, **18**, 1045.
- [2] TODD, B. D., and DAVIS, P. J., 1998, *Phys. Rev. Lett.*, **81**, 1118.
- [3] TODD, B. D., and DAVIS, P. J., 1999, *Comput. Phys. Commun.*, **117**, 191.
- [4] BARANYAI, A., and CUMMINGS, P. T., 1999, *J. chem. Phys.*, **110**, 42.
- [5] MATIN, M. L., DAVIS, P. J., and TODD, B. D., 2000, *J. chem. Phys.*, **113**, 9122; Erratum, 2001, *ibid.*, **115**, 5338.
- [6] MATIN, M. L., DAVIS, P. J., and TODD, B. D., 2003, *Comput. Phys. Commun.*, **115**, 35.
- [7] DAVIS, P. J., MATIN, M. L., and TODD, B. D., 2003, *J. non-Newtonian fluid Mech.*, **111**, 1.
- [8] ARNOLD, V. I., and AVEZ, A., 1968, *Ergodic Problems of Classical Mechanics* (New York: Benjamin).
- [9] KATOK, A., and HASSELBLATT, B., 1995, *Introduction to the Modern Theory of Dynamical Systems* (Cambridge: Cambridge University Press).
- [10] POLLICOTT, M., 1993, *Lectures on Ergodic Theory and Pesin Theory on Compact Manifolds* (Cambridge: Cambridge University Press).
- [11] LIEM, S. Y., BROWN, D., and CLARKE, J. H. R., 1992, *Phys. Rev. A*, **45**, 3706.
- [12] EVANS, D. J., and MORRIS, G. P., 1990, *Statistical Mechanics of Non-equilibrium Liquids* (London: Academic Press).
- [13] LEES, A. W., and EDWARDS, S. F., 1972, *J. Phys. C*, **5**, 1921.
- [14] EVANS, D. J., 1979, *Molec. Phys.*, **37**, 1745.
- [15] PETRAVIC, J., and EVANS, D. J., 1998, *Molec. Phys.*, **95**, 219.
- [16] TODD, B. D., and DAVIS, P. J., 2000, *J. chem. Phys.*, **112**, 40.
- [17] MCCAULEY, J. L., 1997, *Classical Mechanics: Transformations, Flows, Integrable and Chaotic Dynamics* (Cambridge: Cambridge University Press).